Author/s:
Lord, MS;Farrugia, BL;Yan, CMY;Vassie, JA;Whitelock, JM

Title:
Hyaluronan coated cerium oxide nanoparticles modulate CD44 and reactive oxygen species expression in human fibroblasts

Date:
2016-07-01

Citation:
Lord, M. S., Farrugia, B. L., Yan, C. M. Y., Vassie, J. A. & Whitelock, J. M. (2016). Hyaluronan coated cerium oxide nanoparticles modulate CD44 and reactive oxygen species expression in human fibroblasts. Journal of Biomedical Materials Research Part A, 104 (7), pp.1736-1746. https://doi.org/10.1002/jbm.a.35704.

Hyaluronan coated cerium oxide nanoparticles modulate CD44 and reactive oxygen species expression in human fibroblasts

Megan S. Lord*, Brooke L. Farrugia, Claudia M.Y. Yan, James A. Vassie, John M. Whitelock

Graduate School of Biomedical Engineering, University of New South Wales, Sydney, NSW 2052, Australia.

*Address correspondence to: Megan Lord, Graduate School of Biomedical Engineering, University of New South Wales, Sydney 2052 NSW, Australia; Phone: +61 2 9385-3910; E-mail: m.lord@unsw.edu.au

This is the author manuscript accepted for publication and has undergone full peer review but has not been through the copyediting, typesetting, pagination and proofreading process, which may lead to differences between this version and the Version record. Please cite this article as doi:10.1002/jbm.a.35704.

Abstract

Cerium oxide nanoparticles are being widely explored for cell therapies. In this study, nanoceria was functionalized with hyaluronan (HA) using the organosilane linker, 3-aminopropyltriethoxysilane. HA-nanoceria was found to be cytocompatible and to reduce intracellular reactive oxygen species in human fibroblasts. The HA-nanoceria was found to colocalize with CD44 on the surface of the cells and once internalized traffic to the lysosomes, be degraded and induce markers of autophagy. These particles were also effective in reducing the cell surface expression of CD44. Together these data suggest that HA-nanoceria is a promising drug delivery material to target CD44-expressing cells through a variety of mechanisms.

1. Introduction

Cerium oxide nanoparticles (nanoceria) are of interest in therapeutic applications due to their antioxidant properties and potential to deliver drugs to target cell types [1-3]. High levels of intracellular reactive oxygen species (ROS) can lead to oxidative stress and even apoptosis [4]. Many nanomaterials induce ROS leading to cell and tissue damage [5-7]. Nanoceria, however, reduce intracellular ROS once internalized, and are not cytotoxic enabling them to reside within cells and scavenge ROS. These therapeutic properties of nanoceria have been exploited for applications in retinal degeneration and radiation protection [8-10]. Nanoceria possess their anti-oxidant properties through facile cyclic oxidation states that switch between Ce^{3+} and Ce^{4+} [11]. The antioxidant properties of nanoceria are optimal at physiological pH, while at acidic pH the nanoceria behave as oxidases [12]. such as when localized to the lysosomes of cells [1].

Nanoceria have been functionalized with polymers to improve cell-selectivity, stability and also to control their intracellular distribution. Poly(ethylene glycol) functionalization of nanoceria enhances the haemocompatibility of the particles as well as increases residence time and improves stability in suspension [13,14]. Nanoceria have also been functionalized with biological polymers including heparin, which increases uptake and ROS scavenging in a range of cell types, while high levels of heparin functionalization reduce cell proliferation [1,15,16].

Hyaluronan (HA) is a large linear, non-sulphated glycosaminoglycan composed of glucuronate and N-acetylglucosamine that plays a role in many biological processes including cell growth, inflammation, tumor development and wound repair [17-19]. HA also acts as a lubricant and shock absorber in cartilage. Cells react specifically with HA through a range of cell surface receptors, the main being cluster of differentiation 44 (CD44) [20]. CD44

is overexpressed on the surface of many cancer cell types with different splice forms of CD44 being present on different cell types [21]. CD44 is involved in regulating cell proliferation, migration and metastatic processes [22,23]. For this reason variants of CD44 have been explored as diagnostic or prognostic markers of some tumors and reagents interfering with CD44-ligand interactions are being explored to treat these tumors [24-26]. Cancer associated fibroblasts also express CD44 and play a role in cancer cell survival and stemness, suggesting that targeting these cells through CD44 might be an effective cancer treatment strategy [27].

Nanoparticles have been functionalized with HA as a strategy for targeted drug delivery. For example, paclitaxel- phosphatidylethanolamine clusters coated with HA were delivered selectively to tumors based on CD44 expression [28]. Iron oxide nanoparticles functionalized with HA were internalized to a larger extent than the iron oxide particles alone [29]. The size of the HA that is functionalized to the surface of nanoparticles modulates the affinity for CD44 with larger HA fragments having a higher affinity than the smaller HA fragments [30].

As CD44 participates in the uptake and intracellular degradation of HA [21] we hypothesized that HA functionalized nanoceria would exhibit enhanced uptake compared to nanoceria in cells expressing CD44 and that the cells would degrade the HA on the nanoceria to enable intracellular ROS scavenging. Hence, the aims of this study were to functionalize nanoceria with HA and to investigate the biological activity of these particles in terms of cell viability, uptake, ROS scavenging and intracellular localization in fibroblast cells expressing CD44.

2. Materials and Methods

Chemicals were purchased from Sigma-Aldrich (Castle Hill, Australia) unless stated otherwise.

2.1. Synthesis and characterization of nanoceria functionalized with HA

Nanoceria were synthesized using flame spray pyrolysis as described previously [31] with liquid precursor and sheath gas flow rates of 5 mL/min each which resulted in nanoceria with a diameter of 7 nm as estimated by measuring the specific surface area. Nanoceria were functionalized with HA through an organosilane linker, 3-aminopropyltriethoxysilane (APTES). A highly purified pharmaceutical preparation of HA derived from cockerel combs (170,000 average molecular weight) was kindly provided by Dr. James Melrose (Kolling Institute of Medical Research, University of Sydney, Australia) and obtained from Fidia (Abano Terme, Italy) [32]. Nanoceria were dispersed in dimethylformamide at a concentration of 10 mg/mL and sonicated for 2 h at 45^{o}C. APTES (250 μL, 1.07×10^{-3} mol) was added drop-wise to the nanoparticle suspension and stirred for 24 h at 45 ^{o}C. The APTES modified particles were washed three times with toluene followed by one wash with acetone. Particles were then dried for 16 h in a fume hood before vacuum drying at 40^{o}C for 16 h. HA was dissolved in a 1:1 dimethylsulfoxide (DMSO)/water mixture (10 mL) to generate a theoretical 10% coverage of the nanoceria surface. 1-Ethyl-3-(3-dimethylaminopropyl)-carbodiimide (EDC, 2.57×10^{-3} g, 1.34×10^{-5} mol) and N-hydroxysuccinimide (NHS, 1.35×10^{-2} g, 1.17×10^{-4} mol) were then added to the above mixture and stirred at 50 °C for 6 h. The HA-NHS was added to the suspension containing APTES-nanoceria (200 mg) in 1:1 DMSO/water mixture and stirred for 3 days at ambient temperature. The HA-APTES-nanoceria was purified by washing with 1:1 DMSO/water mixture four times. Acetone was used for the final wash to facilitate the removal of DMSO and water. The particles were first air dried in a fume hood for 16 h and later transferred to a vacuum oven for further drying at 40 °C for 16 h. Nanoparticle suspensions were prepared by weighing particles in powder form and resuspending in a defined volume using a sonicator probe immediately prior to use.

High resolution transmission electron microscopy (HR-TEM) of the nanoceria was performed using a Philips CM200 operating at 200 kV with a SIS CCD camera. The level of HA functionalization was determined using a thermogravimetric analyzer (TGA) 2950HR V5.4A operating in an air atmosphere with a heating rate of 5 °C/min between 20 and 1000 °C. The number of molecules attached to the nanoparticles was determined by applying the formula, $N = \frac{XN_A\rho V}{MW}$, where N is the number of molecules on each nanoparticle, X is the percentage weight loss, N_A is Avogadro's number, ρ is the density of the nanoparticle and V is the volume of one nanoparticle and MW is the molecular weight of the molecule. A Perkin Elmer Spotlight 400 Attenuated total reflectance-Fourier transform infra-red spectroscopy (ATR-FTIR) was used to measure changes in the surface chemical structure of the nanoceria following functionalization with APTES and HA. Spectra were recorded between 650 and 4000 cm^{-1}. The hydrodynamic radius and zeta potential of the HA-nanoceria, APTES-nanoceria and nanoceria were obtained using a Malvern Zetasizer Nano-ZS instrument (4 mV laser, λ = 632 nm) after exposure of the particles to cell culture medium for 2 h. Samples were filtered using a 0.45 µm filter prior to analysis at 25 °C. Five measurements were performed per sample.

2.2. Culture of human fetal lung fibroblast cells

The human fetal lung fibroblast cell line, MRC5, was cultured in Dulbecco's Modified Eagle's Medium (DMEM) culture medium containing 10% (v/v) fetal bovine serum, 100 U/mL penicillin and 100 µg/mL streptomycin in a humidified incubator (5% CO_2/95% air atmosphere at 37 °C).

2.3. Cell viability analysis

Fibroblasts were seeded in 96-well tissue culture polystyrene plates at a density of 1.5 × 10^4 cells/well in 200 µL medium. Cells were incubated for 4 h prior to the addition of nanoceria, APTES-nanoceria or HA-nanoceria at a concentration of 50 µg/mL or 1.225

μg/mL HA, which is equivalent to the amount of HA present in 50 μg/mL HA-nanoceria. Cell viability was analyzed at 24, 48 and 72 h using the CellTiter 96® AQueous One Solution Cell Proliferation assay. The CellTiter 96® AQueous One Solution reagent (Promega, Madison, USA) was added to the cell cultures 6 h prior to measurement of the absorbance at 490 nm. Cells exposed to medium only were used as a positive control for the assay. Background absorbance readings were also obtained for each of the treatments in the absence of cells and indicated that the materials themselves did not alter the background absorbance level.

2.4. Intracellular ROS and nanoparticle uptake analysis

The level of cellular ROS was measured using the intracellular peroxide-dependent oxidation of 2', 7'-dichlorodihydrofluorescein diacetate (DCFH-DA) to form a fluorescent compound, 2', 7'-dichlorofluorescein (DCF). Fibroblasts were seeded in 12-well tissue culture polystyrene plates at a density of 5×10^4 cells/well in 1.5 mL medium and incubated for 5 h prior to the addition of 50 μg/mL nanoceria, APTES-nanoceria or HA-nanoceria or 1.225 μg/mL HA. The presence of ROS was determined at 24, 48 and 72 h after the addition of nanoparticles. Cells exposed to medium only were analyzed at each of the time points to determine the normal level of ROS in the cells. Cells exposed to 4% (w/v) ethanol at each of the time points were used as a control for dead cells and cellular debris for the flow cytometry analysis. Cells were removed from culture dishes by trypsinization and resuspended in Dulbecco's phosphate buffered saline, pH 7.4 (DPBS). Cells were then centrifuged at 1000 rpm for 6 min, the supernatant was removed and cells were resuspended in 1 mL DPBS and were incubated with 10 mM DCFH-DA for 30 min at 37 °C prior to analysis by flow cytometry. For each sample, data was acquired for 10^4 gated events using a flow cytometer (BD FACSort) by measuring fluorescence intensity along with the number of cells. Data were analyzed using the FCS 4 Express software. The level of auto-oxidation of

the DCFH-DA in DPBS or in DPBS supplemented with 50 µg/mL nanoceria was found to be significantly lower than in the presence of cells [15].

Nanoparticle uptake was measured by flow cytometry by measuring side scatter at the same time as intracellular ROS analysis. Side scatter measures the granularity of cells and has been used to analyze nanoceria uptake into cells and/or binding to the cell membrane [1,33]. Nanoparticle uptake was also analyzed by phase contrast microscopy after exposure of the fibroblasts seeded in 12-well tissue culture polystyrene plates at a density of 5×10^4 cells/well in 1.5 mL medium and incubated for 5 h prior to the addition of 50 µg/mL HA-nanoceria, nanoceria or no additives. Cells were imaged by light microscopy (Axioskop Mot Mat 2, Zeiss, Australia) after 24 h of exposure to the particles at 500× magnification.

2.5. Analysis of expression of HA and CD44 by flow cytometry

The expression of HA and CD44 was investigated by flow cytometry after exposure of the fibroblasts to HA-nanoceria or nanoceria. Fibroblasts were seeded in 12-well tissue culture polystyrene plates at a density of 1.5×10^5 cells/ well in 2 mL medium and incubated for 5 h prior to the addition of 50 µg/mL nanoceria or HA-nanoceria or 1.225 µg/mL HA. The levels of HA and CD44 were determined at 24, 48 and 72 h after the addition of nanoparticles Cells were fixed with 4% (w/v) paraformaldehyde for 15 min at room temperature (RT) followed by washing with DPBS. Cells were then resuspended in the permeabilizing solution (300 mM sucrose, 50 mM NaCl, 3 mM $MgCl_2$,2 mM HEPES, 0.5 % Triton X-100, pH 7.2) for 5 min on ice, washed with DPBS and centrifuged at 1200 rpm for 5 min. Cells were blocked with 1 % (w/v) bovine serum albumin (BSA) in DPBS for 30 min at RT. 500 µl of cell suspension (5×10^5 cells) was incubated with a rat monoclonal anti-CD44 antibody (clone Hermes-1, AbCam, Cambridge, MA, USA, 1 µg/mL) or 5 µg/mL biotinylated hyaluronan binding protein (bHABP) purified as described previously [34] for 30 min at RT followed by washing with DPBS and centrifugation at 1200 rpm for 5 min to detect HA.

Control samples were prepared by incubating cells with isotype controls, rat IgG (1:500 in 1 % BSA in DPBS). Cells were then incubated with biotinylated rabbit anti-rat IgG (Dako Cytomation Glostrup, Denmark, 1:500 in 1 % BSA in DPBS). Cells were then incubated with streptavidin-fluorescein isothiocyanate (SA-FITC, GE Healthcare, Rydalmere, Australia, 1:500 in 1% (w/v) BSA in DPBS) for 30 min at RT. For each sample, data was acquired for 10^4 gated events using a flow cytometer (BD FACSort) by measuring fluorescence intensity along with the number of cells. Data were analyzed using the FCS 4 Express software.

2.6. Localization of HA, CD44, LC3 and lysosomes by confocal fluorescence microscopy

The expression of HA, CD44 and microtubule-associated protein light chain 3 (LC3) was investigated by confocal fluorescence microscopy after exposure of the fibroblasts to HA- nanoceria, nanoceria, HA or medium. Fibroblasts were seeded in 16-well glass chamber slides at a density of 3×10^4 cells in 200 µL of medium and incubated for 72 h prior to addition of 50 µg/mL of HA- nanoceria, nanoceria or 1.225 µg/mL HA. After incubating for a further 24 to 72 h, cells were rinsed with DPBS then fixed with 4% formaldehyde in DPBS for 15 min at 15 °C, permeabilized at 4 °C with 300 mM sucrose, 50 mM NaCl, 3 mM $MgCl_2$,2 mM HEPES, 0.5% Triton X-100, pH 7.2 for 5 min and blocked in 1% BSA in 50 mM Tris-HCl, 0.15 M NaCl, pH 7.6 (TBS) for 1 h at RT. Samples were rinsed in TBS containing 0.5 (w/v)% Tween-20, pH 7.6 (TBST). Samples that were probed for the presence of HA were incubated with 5 µg/mL bHABP in TBST for 2 h at 37 °C followed by incubation with SA-FITC (1:500 dilution) for 1 h at RT. Samples that were probed for LC3 were incubated with a rabbit polyclonal anti-LC3 antibody (APG8A, Abgent, San Diego, CA, USA, 1:200 dilution) for 2 h at 37 °C followed by incubation with AlexaFluor® 594 conjugated goat anti-rabbit IgG secondary antibody (Life Technologies, Carlsbad, CA, USA, 1:500 dilution) for 1 h at RT. Samples that were probed for CD44 were incubated with a rat monoclonal anti-CD44 antibody (clone Hermes-1, 1 µg/mL) for 2 h at 37 °C followed by

incubation with AlexaFluor® 594 conjugated goat anti-rat IgG secondary antibody (Life Technologies, Carlsbad, CA, USA, 1:500 dilution) for 1 h at RT. Samples were probed for lysosomes using LysoTracker red DND-99 (Life Technologies, Carlsbad, CA, USA, 50 nM) for 30 min at 37 °C prior to fixation. The cytoplasm was stained using 2 µg/mL HSC CellMask orange (Life Technologies, Carlsbad CA, USA) for 30 min at RT. In the final step, slides were rinsed in TBST, incubated for 10 min at 37 °C with 4',6-diamidino-2-phenylindole (DAPI; Life Technologies, Carlsbad, CA, USA, 1 µg/mL) and rinsed again with TBST before mounting with anti-fade reagent. Images were taken with a multiphoton laser scanning confocal microscope (Olympus FV1200, Olympus, Australia). Images were processed using FluoView FV10-ASW 4.1 Viewer (Olympus, Australia) and ImageJ 1.49m. Colocalization was quantified using the Mander's colocalization coefficient (MCC) that provides a measure of co-occurrence of two channels independent of signal proportionality and was reported as the fraction of pixels with positive values in both channels.

2.7. Statistical analysis

A one-way analysis of variance (ANOVA) was performed to compare multiple conditions. Results of $p < 0.05$ were considered significant. Experiments were performed in triplicate and experiments were repeated twice.

3. Results

3.1. Functionalization of cerium oxide nanoparticles with HA

The nanoceria that were synthesized by flame spray pyrolysis were analyzed by HR-TEM and indicated that the particles were rhombohedral-shaped with a high level of crystallinity and well-defined lattice fringes (Figure 1A). HA was covalently bound to the nanoceria through an organosilane linker, APTES. Successful functionalization of the nanoceria was verified by ATR-FTIR (Figure 1B). Conjugation of APTES to the nanoceria

was confirmed by the presence of peaks at 300, 1500 and 1000 cm^{-1} representing the CH_2 stretch, N-H bend and Si-O bond, respectively. The addition of HA to the APTES functionalized particles resulted in a decrease in intensity of the Si-O bond at 1000 cm^{-1} due to the silane group providing a reaction site for the carboxyl groups on HA. Nanoceria were positively charged in cell culture medium at pH 7.4 while functionalization of the surface of the nanoceria with APTES or APTES-HA reduced the overall charge (Figure 1C), however this reduction in zeta potential was not significant indicating that the stability of nanoceria, APTES-nanoceria and HA-nanoceria would be similar. Analysis of the hydrodynamic radius of the particles in cell culture medium confirmed that there was agglomeration of each of the nanoparticles, however the HA-nanoceria formed significantly ($p<0.05$) smaller aggregates than either nanoceria or APTES-nanoceria (Figure 1D).

TGA was used to quantify the amount of APTES and HA that was conjugated to the nanoceria (Table 1). Nanoceria exhibited a weight loss of 4.3% by TGA over the temperature range of 20-1000 °C due to the hydroxyl groups on the surface. The loss in weight of the APTES-nanoceria compared to the nanoceria was 18.4% which equated to approximately 521,400 APTES groups per nanoparticle or 0.85 mmol/g particles. A weight loss of 2.5% was measured for HA- nanoceria compared to APTES-nanoceria which equated to approximately 90 HA molecules bound to each nanoceria or 144 nmol/g particles.

3.2. Cellular interactions with hyaluronan functionalized nanoceria

The effect of HA-nanoceria, APTES-nanoceria and nanoceria on cell proliferation was analyzed with human fetal fibroblast cells exposed to the nanoparticles at a concentration of 50 μg/mL and compared to HA alone at an equivalent concentration to that present in the HA-nanoceria (1.225 μg/mL HA) over a period of 72 h. None of the test conditions reduced cell proliferation over the 72 h analysis period compared to cells exposed only to culture medium (Figure 2).

Intracellular ROS levels were measured by flow cytometry after exposure of the fibroblasts to either culture medium alone or the addition of HA-nanoceria, APTES-nanoceria, nanoceria or HA for a period of 72 h (Figure 3). Presentation of the data as mean fold change in DCF signal compared to cells exposed to medium only after correction for the level of DCF fluorescence in dead cells and cellular debris indicated that cells exposed to APTES-nanoceria displayed 72, 67 and 60% of the level of intracellular ROS of cells exposed to medium only at the 24, 48 and 72 h time points, respectively (Figure 3). Similarly, cells exposed to HA-nanoceria experienced 41, 46 and 26% of the level of intracellular ROS of cells exposed to medium only at the 24, 48 and 72 h time points, respectively (Figure 3). In contrast, cells exposed to nanoceria experienced 74, 62 and 57 % of the level of intracellular ROS of cells exposed to medium only at the 24, 48 and 72 h time points, respectively (Figure 3). This indicated that HA-nanoceria significantly reduced ($p < 0.05$) intracellular ROS compared with cells exposed to nanoceria at all time points (Figure 3). HA alone did not significantly change the level of intracellular ROS compared with cells exposed to medium only at any of the time points (Figure 3).

Uptake of the HA-nanoceria into fibroblasts was analyzed over 72 h by flow cytometry using the side scatter parameter that indicated the granularity of the cells (Figure 4). Both HA-nanoceria and nanoceria significantly increased ($p < 0.05$) the side scatter of the cells. This indicated that these nanoparticles were internalized by or bound to the cell membrane of the fibroblasts at each of the time points tested, with the extent of internalization/cell surface binding increasing from the 24 to 48 h time point and decreasing at the 72 h time point relative to the medium only control. The side scatter measurements for HA-nanoceria were significantly increased ($p < 0.05$) after both 48 and 72 h of exposure compared to cells exposed to nanoceria indicating that the HA functionalization facilitated enhanced uptake of the nanoparticles into cells and/or binding to the cell membrane.

Exposure of cells to HA did not increase the side scatter of the cells compared to cells exposed to medium only over the 72 h analysis period (Figure 4) as HA internalization is not expected to alter the granularity of the cells.

Uptake and/or binding of HA-nanoceria and nanoceria to the plasma membrane was also observed by light microscopy after 24 h of exposure to the particles. Enhanced levels of cell-associated and/or internalized HA-nanoceria were observed compared with nanoceria (Figure 5A and B), thus confirming the flow cytometry data. Additionally, aggregates of both HA-nanoceria and nanoceria were observed in the medium surrounding the cells that were not present in the medium only control (Figure 5 A and B). The intracellular localization of the HA-nanoceria was confirmed by confocal fluorescence microscopy by probing for the localization of HA compared to the cytoplasm and imaging an intracellular focal plane. HA-nanoceria were localized intracellularly with no appreciable change in the extent of uptake over the 72 h analysis period (Figure 5 D-F).

Uptake of the HA-nanoceria was analyzed by confocal fluorescence microscopy to distinguish between particles internalized by the cells and those bound to the cell surface. This was performed by staining cells for the presence of HA, cytoplasm and nuclei after exposure of the cells to the HA-nanoceria, nanoceria or HA for 24 h at a concentration of 50 μg/mL and imaging an intracellular focal plane. HA was localized intracellularly and pericellularly in cells that had been exposed to each of the treatment conditions. HA expression was elevated in cells exposed to HA-nanoceria compared to cells exposed to each of the other conditions consistent with the uptake of the HA-nanoceria (Figure 6). Additionally, HA expression was elevated in cells exposed to HA compared to cells exposed to nanoceria or medium (Figure 6 B-D). Nanoceria did not alter the intracellular level of HA compared to cells exposed to medium only (Figure 6B).

Cells exposed to HA-nanoceria over the 72 h analysis period exhibited enhanced levels of cell associated HA compared with cells exposed to medium only (Figure 7A and B). In contrast, cells exposed to either nanoceria or HA after both 24 and 48 h did not exhibit enhanced levels of cell associated HA compared with cells exposed to medium only. However, after 72 h of exposure to nanoceria or HA cells exhibited a 1 and 2 % increase in HA levels, respectively. Interestingly, cells exposed to HA-nanoceria, nanoceria or HA exhibited 21, 8 and 5% increased levels of HA compared with cells exposed to medium only, respectively (Figure 7C). These data also suggested that the fibroblasts had internalized the HA-nanoceria.

One of the major cell surface receptors for HA is CD44, so it was of interest to determine the cell surface expression of CD44 on cells exposed to HA-nanoceria and nanoceria (Figure 8). Exposure of the cells to either HA-nanoceria or nanoceria reduced the expression of CD44 at each of the time points analyzed compared with cells exposed to medium only. Exposure of cells to HA alone had no effect on the level of CD44 expression over the 72 h analysis period compared with cells exposed to medium only.

Colocalization of HA with CD44, lysosomes and LC3 was investigated using the Mander's colocalization coefficient (MCC) that determines the fraction of pixels with positive values in both channels, independent of signal proportionality. HA was found to colocalize with CD44 to a high degree in cells exposed to nanoceria, HA and medium for 24 h indicating that the HA synthesized by the cells was predominantly localized with CD44 on the cell surface. There was a significant (p<0.05) reduction in HA and CD44 colocalization in cells exposed to HA-nanoceria at 24 h indicating that while some of the HA-nanoceria was localized to the cell surface, much of the HA-nanoceria was internalized by the cells (Figure 9A). After both 48 and 72 h there was a significant (p < 0.05) reduction in the level of colocalization between CD44 and HA for cells exposed to nanoceria, HA and medium

compared with their respective levels of colocalization at 24 h. There was no change in the level of CD44 and HA colocalization for cells exposed to HA-nanoceria throughout the 72 h analysis period (Figure 9A). Colocalization of CD44 and HA was widely distributed on the cell surface for cells exposed to each of the conditions (Figure 9D (i)-(iii)).

Colocalization of HA and lysosomes was identified in each of the conditions with cells exposed to HA-nanoceria exhibiting significantly ($p < 0.05$) higher levels of colocalization than cells exposed to each of the other conditions over the 72 h analysis period (Figure 9B). Interestingly, colocalization of HA and lysosomes was significantly ($p < 0.05$) decreased at 48 and 72 h compared with the 24 h time point. Colocalization of lysosomes and HA was widely distributed in cells exposed to each of the conditions (Figure 9D (iv)-(vi)).

LC3 is a cytosolic protein under basal conditions that translocates to the lipid membrane of autophagosomes during autophagy, which is a lysosomal-based degradative pathway that occurs during cell homeostasis and is upregulated during cell stress such as a result of starvation [35,36]. Colocalization of HA and LC3 was also identified in each of the conditions with cells exposed to HA-nanoceria exhibiting significantly ($p < 0.05$) higher levels of colocalization than cells exposed to each of the other conditions after 24 h (Figure 9C). Cells exposed to either HA-nanoceria and nanoceria at both 48 and 72 h resulted in significantly ($p < 0.05$) higher levels of colocalization than at the 24 h time point. Under basal conditions LC3 is diffuse and distributed throughout the cytoplasm, as observed for cells exposed to medium only (Figure 9D (ix)), while during autophagy the localization pattern of LC3 changes to punctuate as observed for cells exposed to HA-nanoceria and nanoceria (Figure 9D (vii) and (viii)).

4. Discussion

In this study nanoceria was successfully functionalized with HA using an organosilane linker, APTES, which has been used previously to functionalize nanoceria with heparin [15]. The nanoceria used in this study possessed a primary particle size of 7 nm, yet when exposed to cell culture medium formed aggregates in the order of 200 nm in diameter. While HA-nanoceria was also prone to agglomeration, it formed much smaller aggregates than nanoceria in cell culture medium in the order of 100 nm in diameter. However, larger aggregates were visible by light microscopy when the particles were incubated with cells in culture medium for longer time periods. Nanoceria has been reported to accumulate in the liver [37] which is not desirable for clinical translation of these nanoparticles as accumulation in the liver results in rapid clearance. Stable nanoparticles less than 100 nm in diameter have been reported to have a longer circulation half-life and reduced clearance through the liver [38]. This indicates that the HA-nanoceria possess aggregate size characteristics that will enable longer circulation times compared to the nanoceria, however this remains to be verified *in vivo*. Particles in the size range up to 200 nm in diameter have been reported to be readily internalized by non-phagocytic cells, however at reduced rates of internalization compared to nanoparticles in the range of 50 – 100 nm [39]. Studies on a range of nanoparticles have found maximum cell uptake in the size range of 30 – 50 nm [40]. In this study HA functionalization enhanced uptake compared to nanoceria indicating that size and surface charge play a role in the extent and kinetics of nanoparticle uptake. Nanoceria and HA-nanoceria used in this study were found not to be cytotoxic to human fetal fibroblast cells. The cyto-compatibility of the nanoceria found in this study is in agreement with many studies investigating cerium oxide nanoparticles produced by both flame spray pyrolysis and wet chemical synthesis techniques [1,2,9,11,15,31]. While the size of nanoparticles can affect their toxicity once internalized by cells, nanoceria are widely reported to possess low cytotoxicity [41].

The HA-nanoceria analyzed in this study reduced intracellular ROS levels in the fibroblast cells to a greater extent than the nanoceria. This indicated that the functionalization with HA did not mask the natural ROS scavenging properties of the nanoceria. HA alone had no effect on the intracellular ROS levels and has also been reported previously for human epithelial cells [42]. Thus the enhanced ROS scavenging of the HA-nanoceria compared to the nanoceria is likely due to the enhanced uptake of the HA-nanoceria compared with the nanoceria. Heparin-nanoceria have also been shown to enhance uptake into cells resulting in enhanced ROS scavenging [15]. ROS depolymerize HA and chondroitin sulfates [43], however enhanced levels of intracellular HA were shown by flow cytometry for cells exposed to the HA-nanoceria further demonstrating that the particles were effective in reducing intracellular ROS. Low concentrations of ROS play a role in many cell signal transduction pathways including the control of cell proliferation and differentiation, while high levels of ROS can be damaging to cell components and induce apoptosis and necrosis [44]. The HA-nanoceria and nanoceria used in this study were effective in reducing the intracellular levels of ROS, however, this was not to the level that affected the cellular signal transduction pathways as cell proliferation was not affected.

CD44 is the main receptor for HA thus it was of interest to determine whether HA functionalization of the nanoceria enhanced uptake in the cells. Indeed the HA-nanoceria was internalized to a greater extent over the 72 h analysis period compared to the nanoceria. Functionalization of nanoceria with other biological molecules has previously been shown to enhance uptake into cells such as with heparin [1]. HA has been used to enhance uptake of nanomaterials and drugs into cells such as HA-chitosan composite hydrogels [45], HA liposomes [46] and doxorubicin containing polylactide-*co*glycolide nanoparticles [47]. There was reduced expression of HA for cells exposed to HA-nanoceria at the 72 h time point indicating that the HA on the nanoceria had started to degrade as there was no change in the level of

HA-nanoceria internalization measured by flow cytometry. Fibroblasts are known to produce hyaluronidases that are secreted as well as stored intracellularly [48], indicating that the cells possess the capability to turn over the HA attached to the nanoceria. Interestingly, the expression of HA was slightly enhanced after 72 h of exposure of cells to either nanoceria or HA, however the reasons for this remain to be determined.

CD44 is involved in binding and internalizing peri-cellular HA [49,50] through proteolytic cleavage that enables the intracellular domain to translocate to the nucleus and regulate gene transcription and also rapidly transport HA to lysosomes for degradation [51,52]. In this study CD44 was detected with an antibody, clone Hermes-1, that binds to the HA binding region in the link module of CD44 in the extracellular region [53,54]. Analysis by flow cytometry indicated that cells exposed to either HA-nanoceria or nanoceria exhibited decreased expression of this region of CD44. This data suggests that treatment of the cells with HA-nanoceria or nanoceria resulted in CD44 cleavage releasing the extracellular region while the intracellular region assisted in the internalization of the HA-nanoceria. Alternatively, the data suggest that nanoceria directly affected the expression of CD44. CD44 expression is controlled by a variety of cytokines including interleukin 1β and epidermal growth factor [55,56]. Nanoceria themselves can downregulate a variety of cytokines including epidermal growth factor [57] and members of the interleukin family of cytokines, suggesting that the reduced expression of these cytokines may downregulate CD44 expression as observed in this study. Confocal microscopy analyses indicated a high level of HA and CD44 colocalization in cells exposed to each of the conditions and reduced colocalization of HA and CD44 for cells exposed to HA-nanoceria. HA can be internalized by receptors other than CD44, such as RHAMM [58], however in this study the high degree of colocalization of CD44 with HA in each of the treatment conditions indicated that CD44 was the dominant receptor for the HA-nanoceria.

The intracellular localization of the HA-nanoceria was investigated with particular emphasis on colocalization of lysosomes as it is a common organelle for engineered nanoparticles to accumulate in within cells. A high degree of colocalization between HA and lysosomes was established for cells exposed to HA-nanoceria indicating that most of the particles were transported to the lysosomes. In contrast, the nanoceria without functionalization have been shown to be distributed throughout the cytoplasm [1,15]. The level of intracellular HA decreased over time for cells exposed to the HA-nanoceria indicating that the cells were processing the HA attached to the nanoceria, most likely in the lysosomes as previously reported [51].

Intracellular HA has been shown to generate a stress response that drives autophagy [59] thus this study also investigated the colocalization of HA with an autophagy marker, LC3. Autophagy is a normal lysosomal-based degradative pathway that occurs during cell homeostasis and is upregulated during cell stress such as a result of starvation [35]. During autophagy intracellular components are engulfed by autophagosomes that then fuse with lysosomes. LC3 is a cytosolic protein under basal conditions that translocates to the lipid membrane of autophagosomes during autophagy [36] resulting in a change in the localization pattern of LC3 from diffuse to punctuate that can be analyzed by microscopy. In this study punctuate LC3 was observed to colocalize with HA in cells exposed to HA-nanoceria indicating that these particles had induced autophagy. In other treatment conditions the LC3 was diffuse throughout the cytoplasm indicating that autophagy had not been induced.

5. Conclusions

This study demonstrated that nanoceria can be functionalized with HA resulting in an engineered nanomaterial that binds to the cell surface receptor CD44 that is expressed on the cell surface of many cells types and is highly expressed by tumor cells and cancer associated

fibroblasts. The HA-nanoceria synthesized in this study was found to be cyto-compatible and reduce intracellular ROS. HA-nanoceria was internalized through the CD44 receptor and trafficked to the lysosomes where HA was degraded. The HA-nanoceria and nanoceria were able to modulate the expression of CD44 suggesting that they are worthy of further investigation to modulate tumor and associated cell proliferation and migration. The fibroblasts also displayed signs of autophagy in response to the HA-nanoceria. In the future these results will be explored further by examining the role of the HA-nanoceria in activating autophagy pathways. Together these data suggest that HA-nanoceria is a promising drug delivery material to treat tumors through a variety of mechanisms.

6. Acknowledgements

This work was supported by funding from the Australian Research Council under the Discovery Project (DP1097149). The authors would also like to acknowledge Dr Wey Yang Teoh (City University of Hong Kong) for preparing the nanoceria and Dr Victor Wong (University of New South Wales) for the use of the TGA.

7. References

1. Lord MS, Tsoi B, Gunawan C, Teoh WY, Amal R, Whitelock JM. Anti-angiogenic activity of heparin functionalised cerium oxide nanoparticles. Biomaterials 2013;34:8808-8818.
2. Karakoti AS, Monteiro-Riviere NA, Aggarwal R, Davis JP, Narayan RJ, Self WT, McGinnis J, Seal S. Nanoceria as Antioxidant: Synthesis and Biomedical Applications. JOM 2008;60:33-37.
3. Hirst SM, Karakoti AS, Tyler RD, Sriranganathan N, Seal S, Reilly CM. Anti-inflammatory properties of cerium oxide nanoparticles. Small 2009;5:2848-56.
4. Martin P, Leibovich SJ. Inflammatory cells during wound repair: the good, the bad and the ugly. Trends Cell Biol 2005;15:599-607.
5. Zhao J, Castranova V. Toxicology of nanomaterials used in nanomedicine. J Toxicol Environ Health B Crit Rev 2011;14:593-632.
6. Schrand AM, Rahman MF, Hussain SM, Schlager JJ, Smith DA, Syed AF. Metal-based nanoparticles and their toxicity assessment. Wiley Interdiscip Rev Nanomed Nanobiotechnol 2010;2:544-68.

7. Soltes L, Mendichi R, Kogan G, Schiller J, Stankovska M, Arnhold J. Degradative action of reactive oxygen species on hyaluronan. Biomacromolecules 2006;7:659-68.
8. Chen J, Patil S, Seal S, McGinnis JF. Rare earth nanoparticles prevent retinal degeneration induced by intracellular peroxides. Nat Nano 2006;1:142-150.
9. Tarnuzzer RW, Colon J, Patil S, Seal S. Vacancy Engineered Ceria Nanostructures for Protection from Radiation-Induced Cellular Damage. Nano Lett 2005;5:2573-2577.
10. Wason MS, Colon J, Das S, Seal S, Turkson J, Zhao J, Baker CH. Sensitization of pancreatic cancer cells to radiation by cerium oxide nanoparticle-induced ROS production. Nanomed-Nanotechnol 2014;9:558-569.
11. Asati A, Santra S, Kaittanis C, Perez JM. Surface-charge-dependent cell localisation and cytotoxicity of cerium oxide nanoparticles. ACS Nano 2010;4:5321-31.
12. Asati A, Santra S, Kaittanis C, Nath S, Perez JM. Oxidase-like activity of polymer-coated cerium oxide nanoparticles. Angew Chem. Int. Ed. 2009;48:2308-2312.
13. Karakoti AS, Singh S, Kumar A, Malinska M, Kuchibhatla SV, Wozniak K, Self WT, Seal S. PEGylated nanoceria as radical scavenger with tunable redox chemistry. J Am Chem Soc 2009;131:14144-5.
14. Qi L, Fresnais J, Muller P, Theodoly O, Berret JF, Chapel JP. Interfacial activity of phosphonated-polyethylele glycol functionalized cerium oxide nanoparticles. Langmuir 2012;28:11448-11456.
15. Ting SRS, Whitelock JM, Tomic R, Gunawan C, Teoh WY, Amal R, Lord MS. Cellular uptake and activity of heparin functionalised cerium oxide nanoparticles in monocytes. Biomaterials 2013;34:4377-4386.
16. Vassie JA, Whitelock JM, Lord MS. Glycosaminoglycan functionalized nanoparticles exploit glycosaminoglycan functions. Methods Mol Biol 2015;1229:557-565.
17. Chen WYJ, Abatangelo G. Functions of hyaluronan in wound repair. Wound Repair Regen 1999;7:79-89.
18. Toole BP. Hyaluronan: From extracellular glue to pericellular cue. Nat Rev Cancer 2004;4:528-539.
19. Jiang D, Liang J, Noble PW. Hyaluronan in tissue injury and repair. Annu Rev Cell Dev Biol 2007;23:435-461.
20. Lesley J, Hyman R, Kincade PW. CD44 and its interaction with extracellular matrix. Adv Immunol 1993;54:271-335.
21. Naor D, Sionov RV, Ish-Shalom D. CD44: Structure, function, and association with the malignant process. Adv Cancer Res. Volume 71; 1997. p 241-319.
22. Penno MB, August JT, Baylin SB, Mabry M, Linnoila RI, Lee VS, Croteau D, Yang XL, Rosada C. Expression of CD44 in human lung tumors. Cancer Res 1994;54:1381-1387.
23. Acharya PS, KMajumdar S, Jacob M, Hayden J, Mrass P, Weninger W, Assoian RK, Pure E. Fibroblast migration is mediated by CD44-dependent TGFβ activation. J Cell Sci 2008;121:1393-1402.
24. Marhaba R, Zöller M. CD44 in cancer progression: Adhesion, migration and growth regulation. J Mol Histol 2004;35:211-231.
25. Naor D, Nedvetzki S, Golan I, Melnik L, Faitelson Y. CD44 in cancer. CRC Cr Rev Cl Lab Sc 2002;39:527-579.
26. Misra S, Heldin P, Hascall VC, Karamanos NK, Skandalis SS, Markwald RR, Ghatak S. Hyaluronan-CD44 interactions as potential targets for cancer therapy. FEBS J 2011;278:1429-1443.
27. Kinugasa Y, Matsui T, Takakura N. CD44 expressed on cancer-associated fibroblasts is a functional molecule supporting the stemness and drug resistance of malignant cancer cells in the tumor microenvironment. Stem Cells 2014;32:145-56.

28. Rivkin I, Cohen K, Koffler J, Melikhov D, Peer D, Margalit R. Paclitaxel-clusters coated with hyaluronan as selective tumor-targeted nanovectors. Biomaterials 2010;31:7106-7114.
29. El-Dakdouki MH, Zhu DC, El-Boubbou K, Kamat M, Chen J, Li W, Huang X. Development of Multifunctional Hyaluronan-Coated Nanoparticles for Imaging and Drug Delivery to Cancer Cells. Biomacromolecules 2012;13:1144-1151.
30. Mizrahy S, Raz SR, Hasgaard M, Liu H, Soffer-Tsur N, Cohen K, Dvash R, Landsman-Milo D, Bremer MG, Moghimi SM and others. Hyaluronan-coated nanoparticles: the influence of the molecular weight on CD44-hyaluronan interactions and on the immune response. J Control Release 2011;156:231-8.
31. Lord MS, Jung M, Teoh WY, Gunawan C, Vassie JA, Amal R, Whitelock JM. Cellular uptake and reactive oxygen species modulation of cerium oxide nanoparticles in human monocyte cell line U937. Biomaterials 2012;33:7915-7924.
32. Melrose J, Numata Y, Ghosh P. Biotinylated hyaluronan: A versatile and highly sensitive probe capable of detecting nanogram levels of hyaluronan binding proteins (hyaladherins) on electroblots by a novel affinity detection procedure. Electrophoresis 1996;17:205-212.
33. Busch W, Bastian S, Trahorsch U, Iwe M, Kühnel D, Meißner T, Springer A, Gelinsky M, Richter V, Ikonomidou C and others. Internalisation of engineered nanoparticles into mammalian cells in vitro: influence of cell type and particle properties. Journal of Nanoparticle Research 2011;13:293-310.
34. Melrose J, Smith S, Ghosh P, Taylor TK. Differential expression of proteoglycan epitopes and growth characteristics of intervertebral disc cells grown in alginate bead culture. Cells Tissues Organs 2001;168:137-46.
35. Azad MB, Chen Y, Gibson SB. Regulation of autophagy by reactive oxygen species (ROS): Implications for cancer progression and treatment. Antioxid Redox Signal 2009;11:777-790.
36. Tanida I, Ueno T, Kominami E. LC3 and autophagy. Methods Mol Biol 2008;445:77-88.
37. Molina RM, Konduru NV, Jimenez RJ, Pytgiotakis G, Demokritou P, Wohlleben W, Brain JD. Bioavailability, distribution and clearance of tracheally instilled, gavaged or injected cerium dioxide nanoparticles and ionic cerium. Environ Sci: Nano 2014;1:561-73.
38. Alexis F, Pridgen E, Molnar LK, Farokhzad OC. Factors Affecting the Clearance and Biodistribution of Polymeric Nanoparticles. Molecular Pharmaceutics 2008;5:505-515.
39. Rejman J, Oberle V, Zuhorn IS, Hoekstra D. Size-dependent internalization of particles via the pathways of clathrin- and caveolae-mediated endocytosis. Biochem J 2004;377:159-69.
40. Shang L, Nienhaus K, Nienhaus GU. Engineered nanoparticles interacting with cells: Size matters. J Nanobiotech 2014;12:5-15.
41. Simko M, Tischler S, Mattsson MO. Pooling and analysis of published *in vitro* data: A proof of concept study for the grouping of nanoparticles. Int J Mol Sci 2015;16:26211-36.
42. Pauloin T, Dutot M, Joly F, Warnet JM, Rat P. High molecular weight hyaluronan decreases UVB-induced apoptosis and inflammation in human epithelial corneal cells. Mol Vis 2009;15:577-583.
43. Rees MD, Hawkins CL, Davies MJ. Hypochlorite and superoxide radicals can act synergistically to induce fragmentation of hyaluronan and chondroitin sulphates. Biochem J 2004;381:175-184.

44. Sun Y, Oberley LW. Redox regulation of transcriptional activators. Free Radic Biol Med 1996;21:335-348.
45. Contreras-Ruiz L, de la Fuente M, Parraga JE, Lopez-Garcia A, Fernandez I, Seijo B, Sanchez A, Calonge M, Diebold Y. Intracellular trafficking of hyaluronic acid-chitosan oligomer-based nanoparticles in cultured human ocular surface cells. Mol Vis 2011;17:279-290.
46. Peer D, Margalit R. Tumor-targeted hyaluronan nanoliposomes increase the antitumor activity of liposomal Doxorubicin in syngeneic and human xenograft mouse tumor models. Neoplasia 2004;6:343-353.
47. Yadav AK, Mishra P, Mishra AK, Mishra P, Jain S, Agrawal GP. Development and characterization of hyaluronic acid-anchored PLGA nanoparticulate carriers of doxorubicin. Nanomedicine 2007;3:246-257.
48. Stair-Nawy S, Csoka AB, Stern R. Hyaluronidase expression in human skin fibroblasts. Biochem Biophys Res Commun 1999;266:268-73.
49. Hascall VC, Majors AK, De la Motte C, Evanko SP, Wang A, Drazba JA, Strong SA, Wight TN. Intracellular hyaluronan: A new frontier for inflammation? Biochim Biophys Acta 2004;1673:3-12.
50. Culty M, Nguyen HA, Underhill CB. The hyaluronan receptor (CD44) participates in the uptake and degradation of hyaluronan. J Cell Biol 1992;116:1055-62.
51. Tammi R, Rilla K, J.-P. P, MacCallum DK, Hogg M, MLuukkonen M, Hascall VC, Tammi M. Hyaluronan enters keratinocytes by a novel endocytic route for catabolism. J Biol Chem 2001;276:35111-35122.
52. Okamoto I, Kawano Y, Murakami D, Sasyama T, Araki N, Miki T, Wong AJ, Saya H. Proteolytic release of CD44 intracellular domain and its role in the CD44 signaling pathway. J Cell Biol 2001;155:755-762.
53. Bendall LJ, James A, Zannettino A, Simmons PJ, Gottlieb DJ, Bradstock KF. A novel CD44 antibody identifies an epitope that is aberantly expressed on acute lymphoblastic leukaemia cells. Immunol Cell Biol 2003;81:311-319.
54. Zöller M. CD44: Can a cancer-initiating cell profit from an abundantly expressed molecule? Nat Rev Cancer 2011;11:254-267.
55. Foster LC, Arkonae BM, Sibinga NES, Shi C, Perrella MA, Haber E. Regulation of CD44 gene expression by the proinflammatory cytokine interleukin-1β in vascular smooth muscle cells. J Biol Chem 1998;273:20341-6.
56. Zhang M, Wang MH, Singh RK, Wells A, Siegal GP. Epidermal growth factor induces CD44 gene expression through a novel regulatory element in mouse fibroblasts. J Biol Chem 1997;272:14139-46.
57. Giri S, Karakoti A, Graham RP, Maguire JL, Reilly CM, Seal S, Rattan R, Shridhar V. Nanoceria: A Rare-Earth Nanoparticle as a Novel Anti-Angiogenic Therapeutic Agent in Ovarian Cancer. PLoS ONE 2013;8:e54578.
58. Nedvetzki S, Gonen E, Assayag N, Reich R, Williams RO, Thurmond RL, Huang JF, Neudecker BA, Wang FS, Turley EA and others. RHAMM, a receptor for hyaluronan-mediated motility, compensates for CD44 in inflamed CD44-knockout mice: A different interpretation of redundency. Proc Natl Acad Sci USA 2004;101:18081-6.
59. Wang A, de la Motte C, Lauer M, Hascall VC. Hyaluronan matrices in pathobiological processes. FEBS J 2011;278:1412-1418.

Table 1. Percent weight loss of APTES-nanoceria and HA-APTES-nanoceria compared to nanoceria measured by TGA over the temperature range 20 – 1000 °C heated at 5 °C/min.

	Weight loss (%)	Number of molecules per nanoceria	
		APTES	HA
Nanoceria	4.3	-	-
APTES-nanoceria	18.4	521,400	-
HA-APTES-nanoceria	20.8	521,400	90

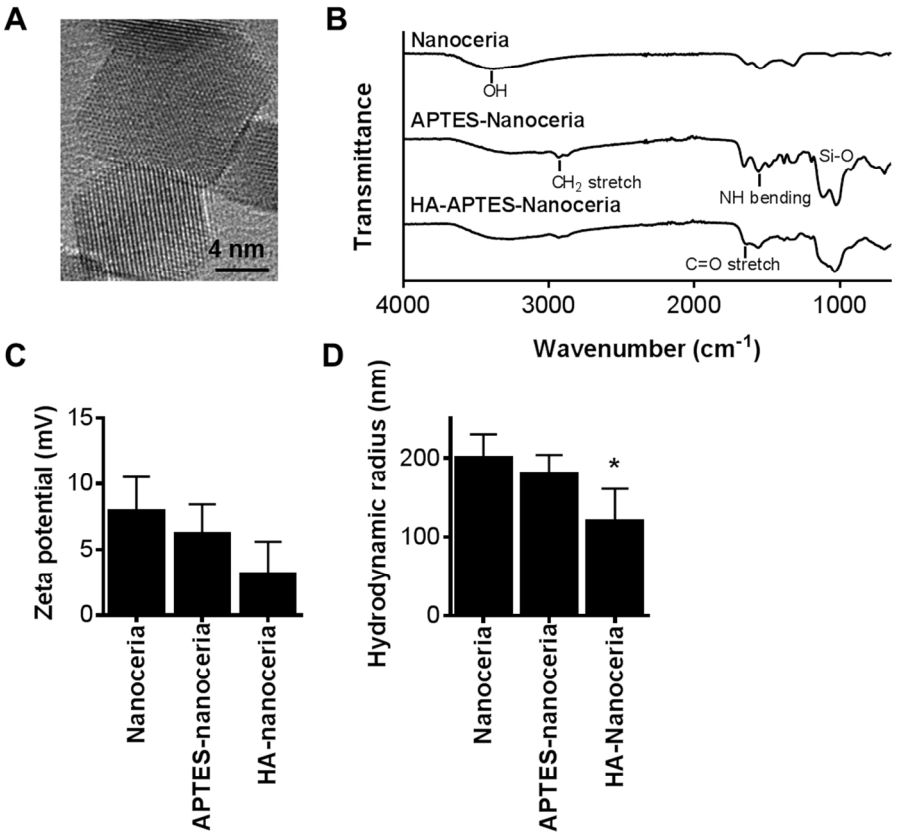

Figure 1. (A) High resolution transmission electron microscopy image of nanoceria with an average particle size of 7 nm; (B) ATR-FTIR spectra of nanoceria, APTES-nanoceria and HA-APTES-nanoceria; (C) zeta potential and (D) hydrodynamic radii of nanoceria and HA-nanoceria in culture medium at pH 7.4. Data presented as mean ± standard deviation (n=5). * indicated significant difference compared to nanoceria ($p<0.05$) analyzed by a one-way ANOVA.
202x183mm (150 x 150 DPI)

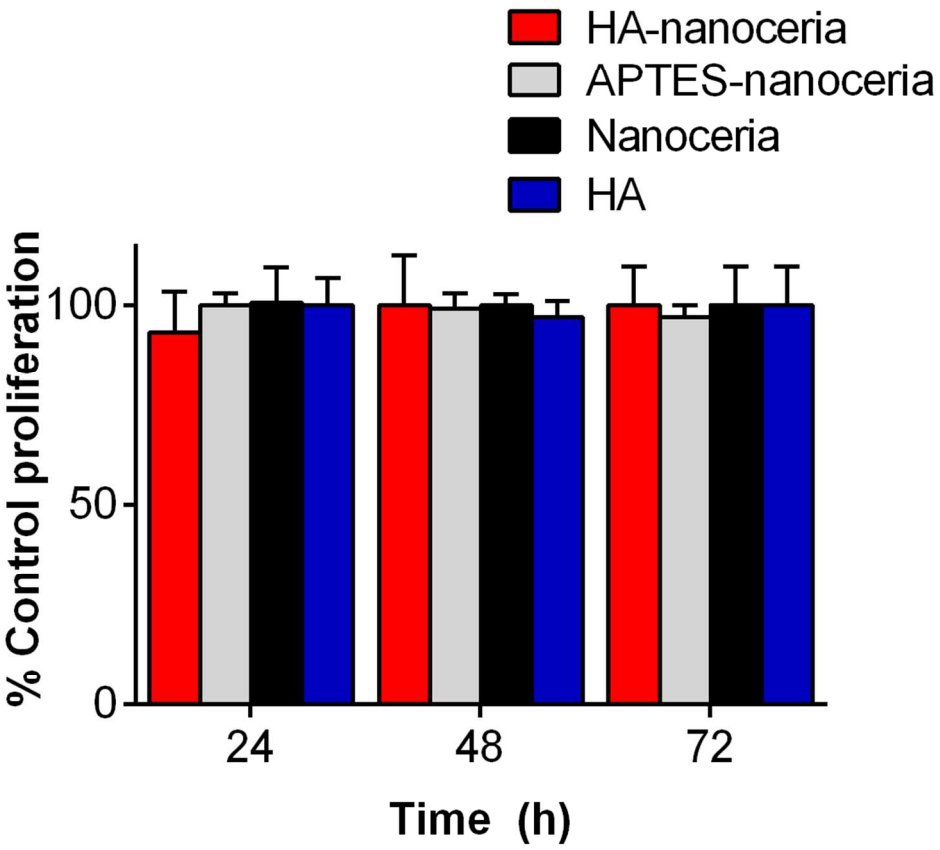

Figure 2. Proliferation of human fetal fibroblasts over a period of 72 h exposed to HA-nanoceria, APTES-nanoceria or nanoceria at a concentration of 50 µg/mL or HA at a concentration 1.225 µg/mL measured by the MTS assay. Data presented at mean ± standard deviation (n =3).
99x90mm (300 x 300 DPI)

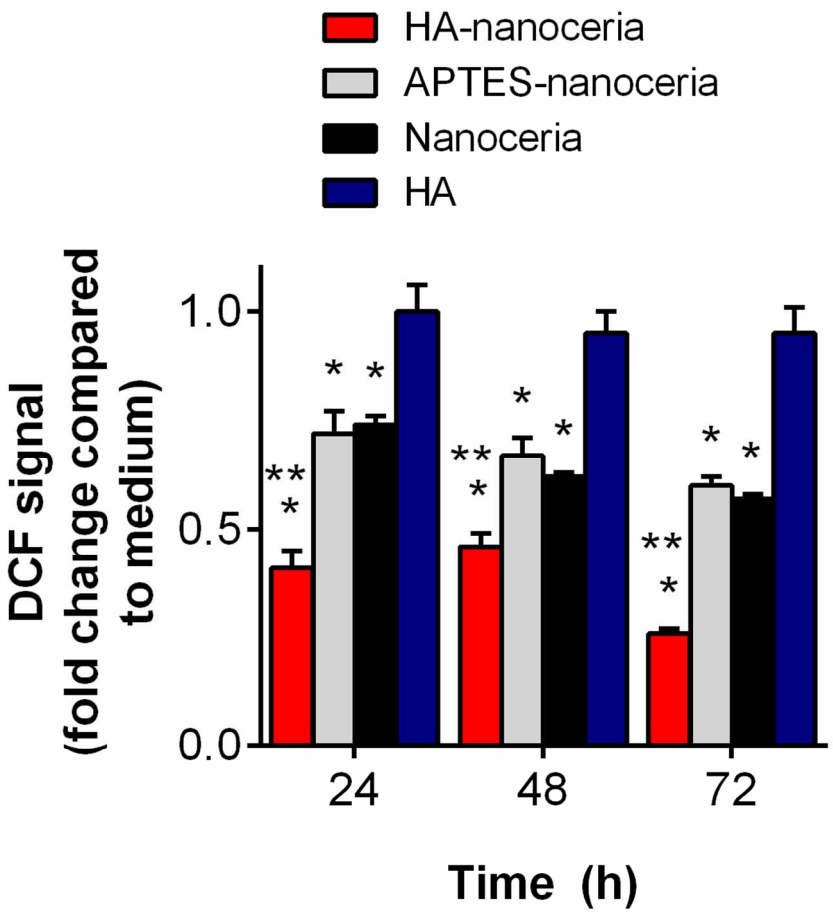

Figure 3. Intracellular ROS levels in human fetal fibroblasts as measured by DCF fluorescence by flow cytometry. Data presented is presented as the mean fold change in DCF signal compared to cells exposed to medium only. Data presented as mean ± SD (n=3). *Indicated significant differences ($p < 0.05$) compared with cells exposed to medium only at each time point as determined by a one-way ANOVA. ** indicated significant reduction ($p < 0.05$) compared with cells exposed to nanoceria at each time point as determined by one-way ANOVA.
106x103mm (300 x 300 DPI)

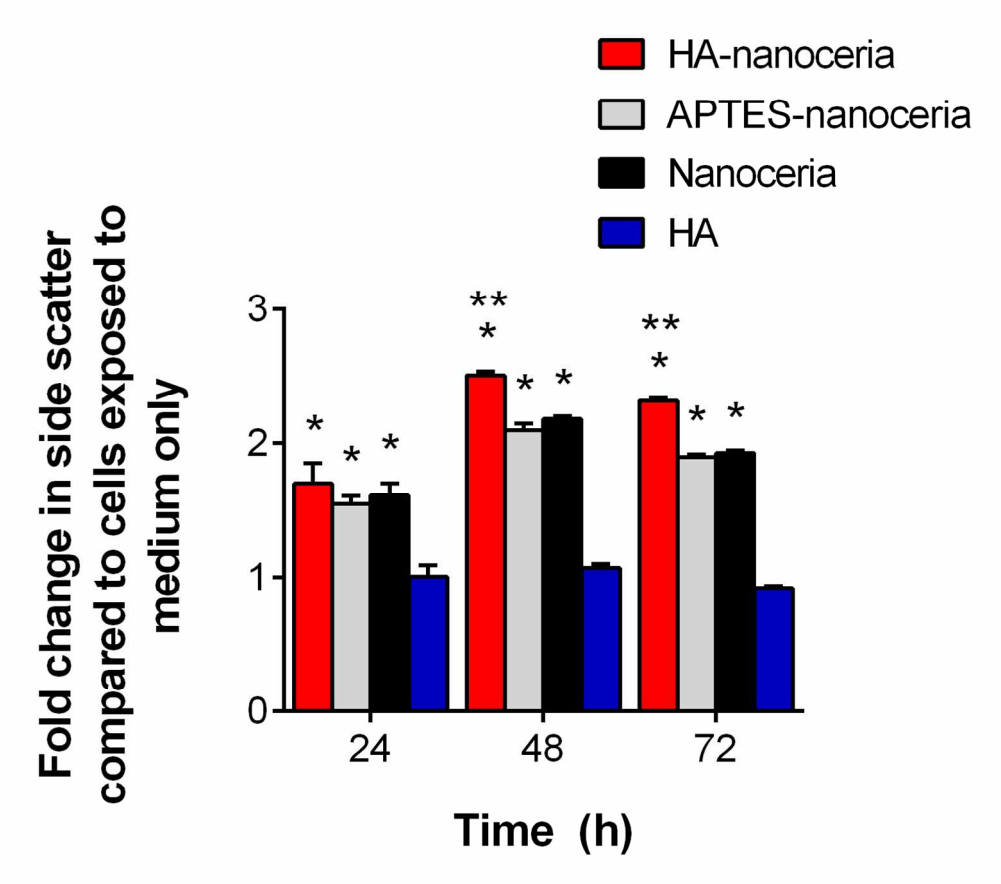

Figure 4. Flow cytometric analysis of HA-nanoceria, nanoceria and HA uptake into human fetal fibroblasts analyzed by side scatter after 24, 48 and 72 h of exposure. Data presented as fold change in side scatter compared to cells exposed to medium only (mean ± standard deviation, n =3). *Indicated significant differences ($p<0.05$) compared with cells exposed to medium only at each time point as determined by a one-way ANOVA. **Indicated significant increase ($p<0.05$) compared with cells exposed to nanoceria at each time point as determined by a one-way ANOVA.
126x111mm (300 x 300 DPI)

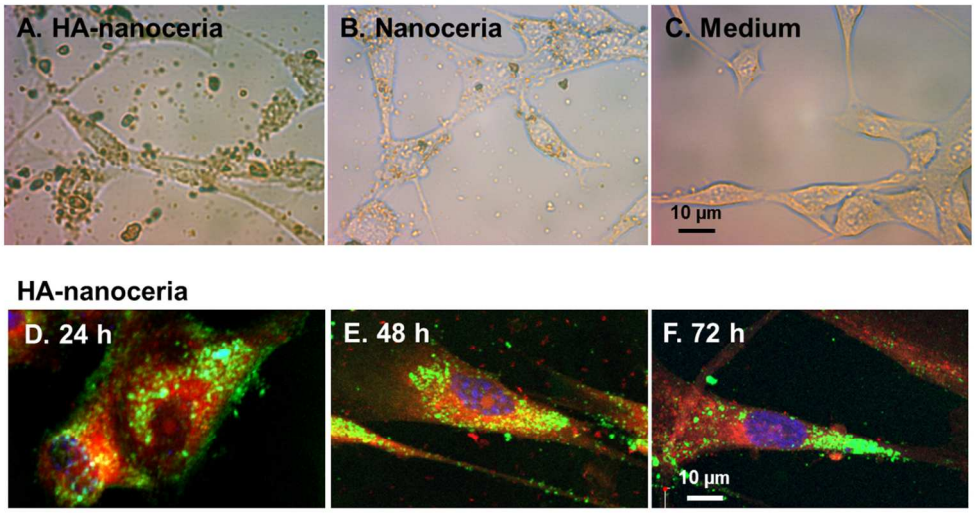

Figure 5. Light microscopy images of human fetal lung fibroblasts exposed to (A) HA-nanoceria, (B) nanoceria or (C) medium for 24 h. Localization of HA (green) in human fetal lung fibroblasts exposed to HA-nanoceria for (D) 24, (E) 48 or (F) 72 h. The cytoplasm (red) and nuclei (blue; (i), (ii) and (iii)) were also stained. Scale bar represents 10 µm.
208x112mm (150 x 150 DPI)

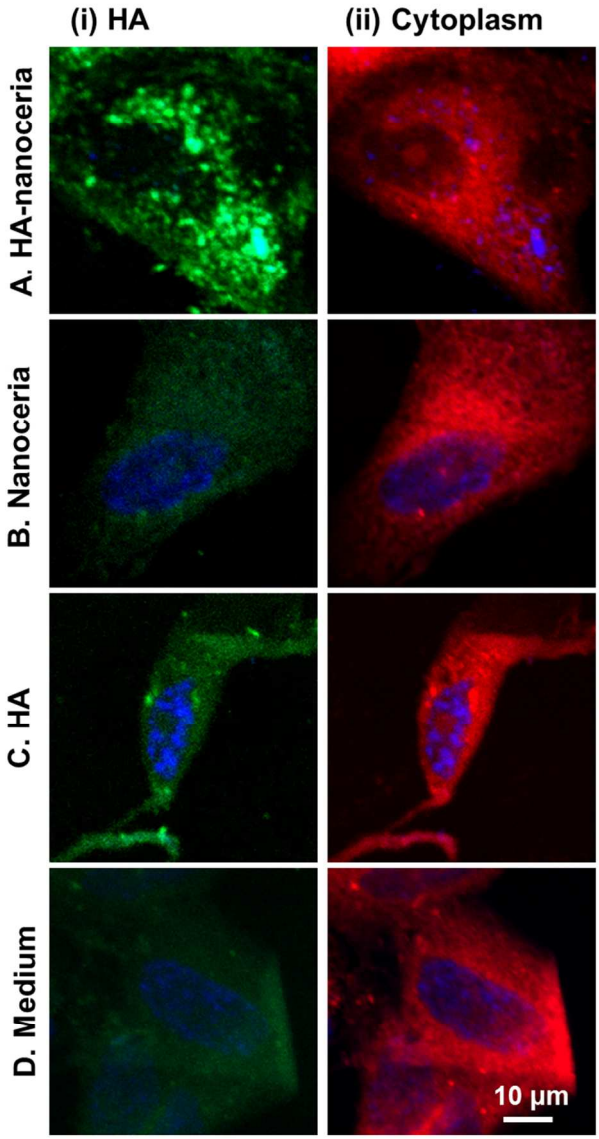

Figure 6. Localization of HA (green) in human fetal lung fibroblasts exposed to (A) HA-nanoceria, (B) nanoceria, (C) HA or (D) medium for 24 h. The cytoplasm (red) and nuclei (blue; (i), (ii) and (iii)) were also stained. Scale bar represents 10 µm.
128x224mm (150 x 150 DPI)

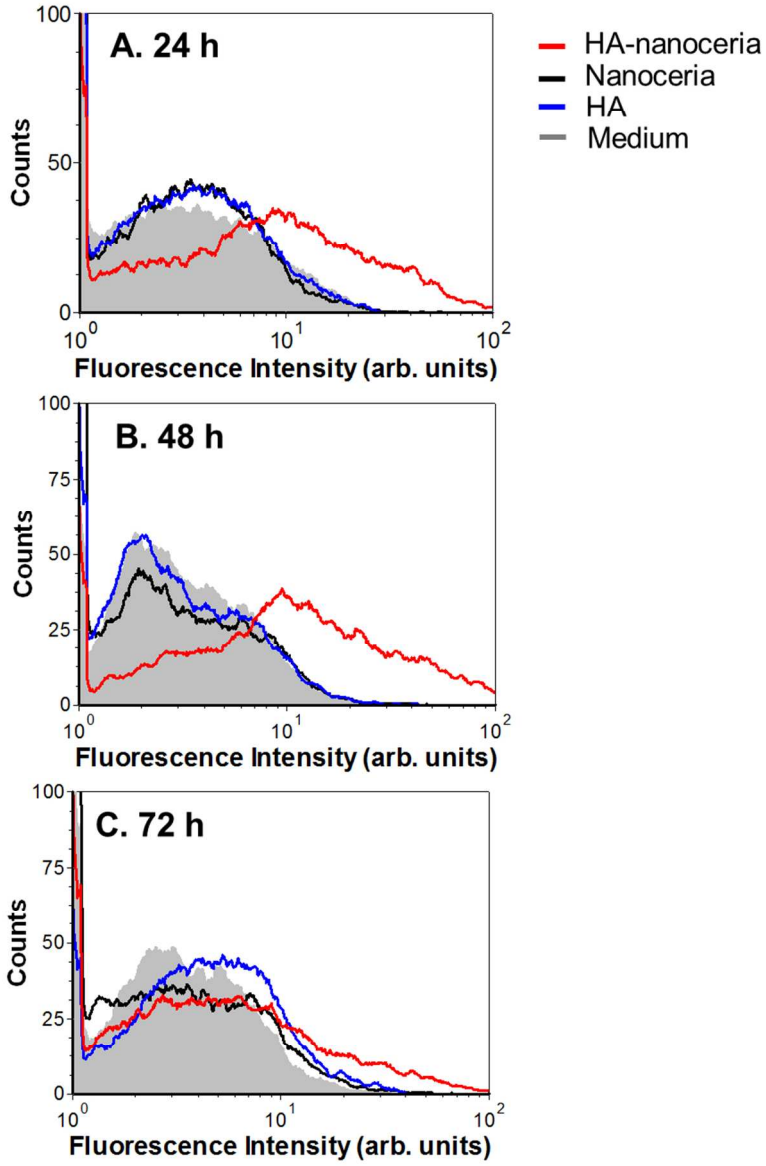

Figure 7. Flow cytometric analysis of the expression of HA at (A) 24, (B) 48 and (C) 72 h after exposure of human fibroblasts to HA-nanoceria, nanoceria or HA compared to cells exposed to medium only. Data presented is representative of all measurements.
150x227mm (150 x 150 DPI)

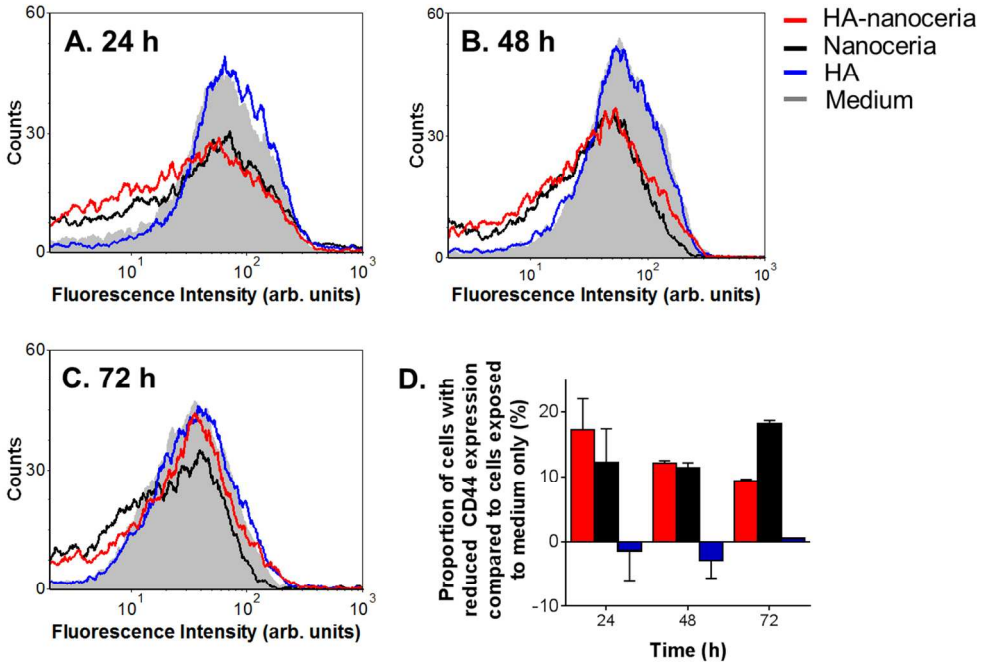

Figure 8. Flow cytometric analysis of the expression of CD44 at (A) 24, (B) 48 and (C) 72 h after exposure of human fibroblasts to HA-nanoceria, nanoceria or HA compared to cells exposed to medium only. Data presented is representative of all measurements. (D) Proportion of cells with reduced CD44 expression compared with cells exposed to medium only at each time point. Data presented as mean ± standard deviation (n=3).
219x155mm (150 x 150 DPI)

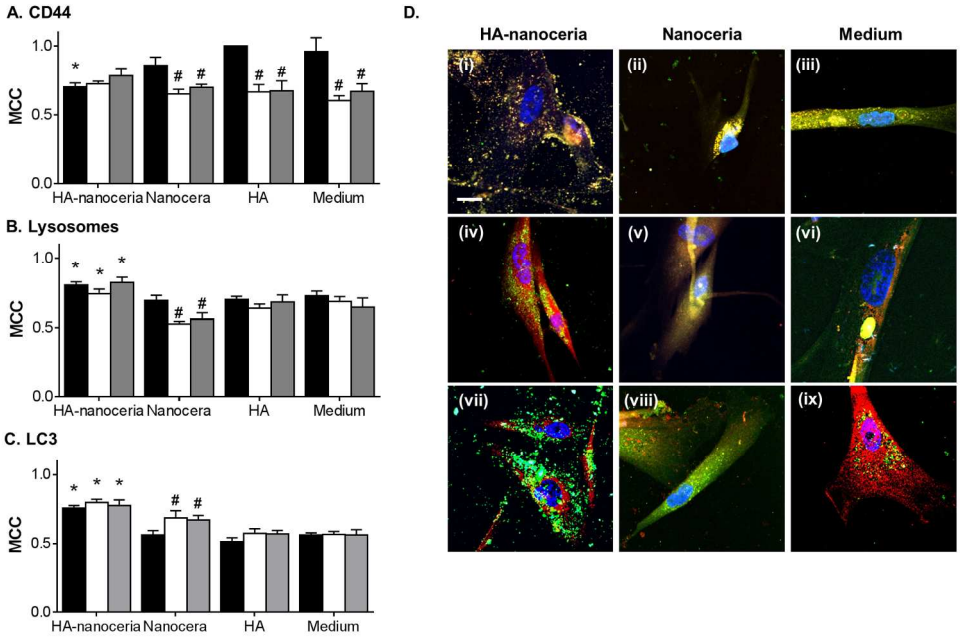

Figure 9. Co-localization of HA with (A) CD44, (B) lysosomes and (C) LC3 as determined by Manders colocalization coefficient (MCC) for cells exposed to HA-nanoceria, nanoceria, HA or medium for 24 (black), 48 (white) and 72 (grey) h. (D) Co-localization if HA (green) and CD44 (red; (i), (ii) and (iii)), lysosomes (red; (iv), (v) and (vi)) or LC3 (red; (vii), (viii) and (ix)) for cells exposed to HA-nanoceria ((i), (iv) and (vii)), nanoceria ((ii), (v) and (viii)) or medium ((iii), (vi) and (ix)) for 24 h. Nuclei shown in blue. Scale bar represents 20 μm. * indicated significant differences compared with cells exposed to medium only at each time point and # indicated significant differences compared within the 24 h time point for each condition as determined by a one-way ANOVA.
332x224mm (150 x 150 DPI)